To be submittet to
Nuovo Cimento

ISTITUTO NAZIONALE DI FISICA NUCLEARE
Laboratori Nazionali di Frascati

LNF-82/50(P)
6 Luglio 1982

M. Belli, A. Bianconi, E. Burattini, S. Mobilio, C.R. Natoli, L. Palladino, A. Reale and A. Scafati:

EXAFS AND XANES STRUCTURE DETERMINATION OF Mn^{2+} BINDING IN ATP COMPLEXES

Servizio Documentazione

INFN - Laboratori Nazionali di Frascati
Servizio Documentazione

LNF-82/50(P)
6 Luglio 1982

EXAFS AND XANES STRUCTURE DETERMINATION OF Mn^{2+} BINDING IN ATP COMPLEXES

M. Belli(°), A. Bianconi(x), E. Burattini(+), S. Mobilio(o), C.R. Natoli(o), L. Palladino(o), A. Reale(*) and A. Scafati(°)

(°) Istituto Superiore Sanità, Laboratori di Fisica and INFN Sezione Sanità, Roma, Italy.

(x) Università di Roma.

(o) Laboratori Nazionali di Frascati dell'INFN, Frascati, Italy.

(*) Laboratori Nazionali di Frascati dell'INFN and Università de L'Aquila, L'Aquila, Italy.

(+) Laboratori Nazionali di Frascati and Università di Napoli, Napoli, Italy.

ABSTRACT

The binding of Mn^{2+} ions to ATP molecules has been studied by means of fine structure analysis of X-ray absorption spectra (EXAFS and XANES) at the K-edge of Mn using the synchrotron radiation facility PULS in Frascati. The results obtained in both freeze-dried and liquid samples of aqueous solutions at room temperature of the Mn-ATP complex under different values of pH and Mn:ATP ratio are reported and discussed.

The Mn^{2+} ion appears to be octahedrally coordinated, the phosphate oxygen atoms being in the first coordination shell. Values of (2.15 ± 0.05) Å and (3.4 ± 0.05) Å respectively have been found for Mn-O and Mn-P distances. Theoretical considerations together with experimental results do not support the existence of a direct binding of the Mn to the N(7) atom and of the adenine ring. The coordination numbers for the first and second shell are consistent with the formation of a $Mn(ATP)_2$ complex in solution at pH=9 and Mn:ATP=1:10, while a Mn ATP 1:1 complex is found at lower pH and higher Mn:ATP ratios.

RIASSUNTO

Il legame Mn^{2+}-ATP è stato studiato mediante analisi della struttura fine dallo spettro di assorbimento alla soglia K del Mn (EXAFS e XANES), utilizzando la radiazione di sincrotrone del PULS di Frascati. Vengono presentati e discussi i risultati ottenuti su campioni, sia liofilizzati che liquidi, di soluzioni a temperatura ambiente del complesso Mn-ATP in diverse condizioni di pH per diversi valori del rapporto Mn:ATP.

Lo ione Mn appare in coordinazione ottaedrica con gli ossigeni dei gruppi fosfati nella prima shell di coordinazione. I valori trovati per le distanze Mn-O ed Mn-P sono di (2.15 ± 0.05) Å e di (3.4 ± 0.05) Å rispettivamente, mentre considerazioni teoriche basate sui risultati sperimentali sembrano escludere la presenza di un legame diretto del Mn con l'N(7) dell'adenina. I numeri di coordinazione per la prima e la seconda shell di coordinazione suggeriscono la formazione di un complesso $Mn\text{-}(ATP)_2$ in soluzione a pH=9 e con Mn:ATP=1:10, mentre a più bassi pH e più alti valori del rapporto Mn:ATP, si trova il complesso Mn-ATP=1:1.

1. - INTRODUCTION

It has been recognized that EXAFS technique is an important tool in biophysics and biochemistry for its application to the analysis of the binding site of metal ions in macromolecular structures in aqueous solution, which cannot be studied by the usual diffraction techniques.

These methods have been first applied to metalloproteins[1]; recently, we used high-resolution X-ray absorption analysis to the study of metal ions binding to nucleotides and nucleic acids.

Metal ions are required for almost all the biological processes in which nucleic acids are involved. Specific complexes with high association constants have been found in nucleic acids, extracted from cells, where Mg^{2+}, Ca^{2+}, Zn^{2+}, Fe^{2+}, Mn^{2+} where the more abundant divalent cations[2,3]. Alterations in the amount or in the nature of metal ions in the living systems may have toxic, mutagenic and carcinogenic effects[2,3,4,5]. Moreover, anomalous amounts of aluminium occur in several human brain deseases[6], some Pt compounds are discovered to have antitumor activity[7] and certain metals have been shown to give protection against radiation damage[8].

There are several lines of evidence indicating that these effects can be described in terms of metal-nucleic acid, or metal-nucleotide, interactions[9].

The 5'-adenosine triphosphate (ATP) molecule, which acts as an activator in several enzymatic reactions, requires the presence of divalent metal ions. The solution structure of metal-ATP complexes is therefore of great importance for their intrinsic biological relevance as well as for their values as simple models for metal-nucleic acid binding. Among the various metal ions, the paramagnetic Mn^{2+} has been the most investigated one, since it can replace Mg^{2+}, giving biologically active Mn-ATP complexes, which can be studied by magnetic resonance techniques[10].

The primary reactive sites for metals in ATP complexes are the negatively charged oxygen atoms of the phosphate groups, and the nitrogen donor atoms of the adenine. A "backbound" phosphate-metal ion - adenine ring complex was proposed by Szent-Gyorgyi[11] in 1957, but some important features of these complexes are still unclear after 25 years of research work. Major controversial points are the nature of metal binding to the ring, and the occurrence of 1:1 or 1:2 metal-nucleotide complexexs in specified conditions.

Binding of Mn to all three phosphates was found by NMR of P-31 nuclei[12]. Since the interaction of Mn also with the adenine ring has been observed by PMR techniques[13], a model was proposed[14] in which Mn^{2+} is octahedrally coordinated to the ATP molecule, where the α, β, γ phosphates and three water molecules are inner-sphere and N(7) of the adenine ring is outer-sphere, the latter interaction being mediated by the H-bond of a water molecule (Fig. 1). On the other hand, further studies have indicated that the metal can bind directly to the N(7) nitrogen[15-16]. The hypothesis of an equilibrium has also been suggested between the 1:1 and the 1:2 (Mn:ATP) complexes; in addition a transition seems to occur on passing from neutral to acids conditions, with

change from an α, β, γ chelation to a β, γ one, resulting from a protonation of the α-phosphate[17]. Thus a quite complicated picture emerges from the body of the experimental results.

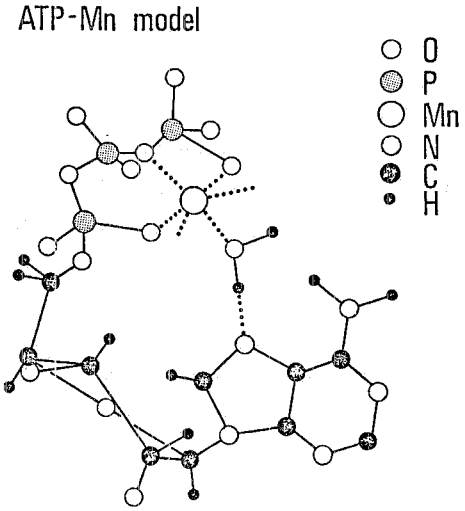

FIG. 1 - A possible structure of Mn-ATP complex, where the metal is octahedrally coordinated. Two water molecules have been omitted for simplicity (Adapted from Ref. (14)).

The present study reports the data on Mn^{2+} site in Mn-ATP complexes, obtained by EXAFS (Extended X-ray Absorption Fine Structure) and XANES (X-ray Absorption Near Edge Structure) measurements.

Our measurements were done also on samples in solution at several pH values in order to look for different site structures favoured by different environment conditions.

2. - METHODS

The X radiation is absorbed, among other processes, by photoelectric effect, and it has long been put in evidence[18] that the photoelectric absorption coefficient rises sharply at the K-edge or L-edge and then varies in a complicate way for energies more than one keV above the edge.

Usually one separates the absorption spectrum in two regions (Fig. 2): the first one around the edge extends up to ~50 eV above the edge, (XANES) and the second one, extending several hundred eV above the absorption

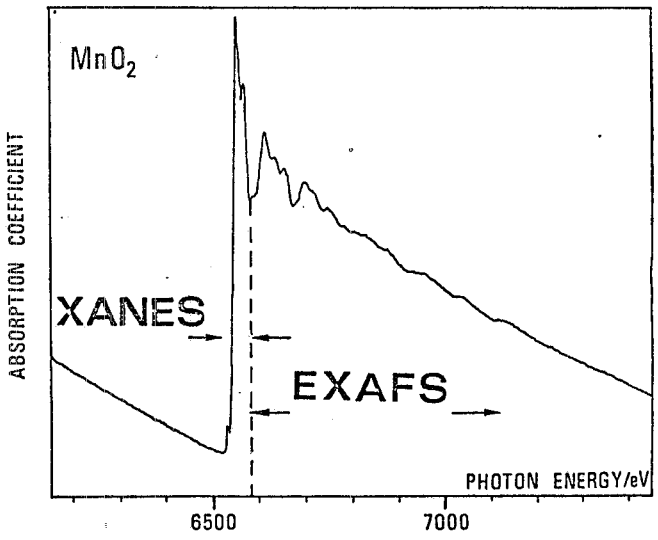

FIG. 2 - Absorption coefficient of a Mn compound (MnO_2) with the indication of XANES and EXAFS regions.

edge, which may display oscillations (EXAFS).

The physical origin of the EXAFS oscillations in the absorption coefficient is due to the final state interference effects, i.e. to the fact that the wave function of the outcoming photoelectron is modified by the presence of the surrounding atoms; the wave function can be described as a superposition of an outgoing wave and electron waves backscattered from neighbouring atoms at the site of the absorbing atom. Therefore the EXAFS analysis gives informations on their relative distance and their nature[19].

In the XANES region one can study unknown local structures, by measuring the dependence of the oscillator strength and energy shift of absorption peaks on the local symmetry and on the chemical binding[20].

Both for EXAFS and XANES regions, the data analysis is usually made by comparing the experimental results with those obtained with some model compound of known microscopic structure.

In the EXAFS region the modulation of the absorption coefficient, normalized to the atomic "background absorption", can be analyzed in terms of a scattering amplitude F(k) from the neighbouring atoms and a phase shift $\phi(k)$ to which both the potential of the absorping atom and of neighbouring atoms contribute.

It has been shown that for the excitation of an S level (K or L edge) the modulating part (k) of the absorption coefficient can be written:

$$\chi(k) = \frac{\mu-\mu_o}{\mu_o} = \Sigma_j A_j(k)\,\mathrm{sen}\,\Psi_j(k), \quad \Psi_j(k) = 2R_j k + \phi_j(k)$$

$$A_j(k) = \frac{N_j}{k R_j^2} \left| F_j(\pi,k) \right| e^{-2\frac{R_j}{\lambda}} e^{-2\sigma_j^2 k^2} \qquad (1)$$

where N_j is the number of atoms at distance R_j in the j-shell around the absorbing atoms, $\left| F_j(\pi,k) \right|$ is the backscattering amplitude from the neighbouring atoms, λ, is the mean free path of the outcoming electron for inelastic scattering losses, and σ^2 is the Debye-Waller factor, which takes into account termal vibration and static disorder.

The photoelectron k wave number is given by

$$k = \left[\frac{2m}{\hbar} (E-E_o) \right]^{1/2} \quad \text{or} \quad \left[k(\mathring{A}^{-1}) = 0{,}262(E-E_o)\,(eV) \right]^{1/2}$$

where E is the photon energy and E_o the threshold energy of the absorption edge.

Several theoretical predictions of phases and backscattering amplitudes have been published, having as starting point the electron-atom scattering process[21].

Two main numerical approaches to data analysis have been developed: Fourier transformations[22] and curve fitting[23]. Both these methods require a detailed knowledge of the amplitude and phase functions to extract the relevant informations as N_j, R_j and σ_j. This is in general achieved by measuring amplitude and phase from EXAFS spectra of known compounds and then using the criterium of "chemical transferability" of these quantities to the unkown samples.

To obtain the difference in the geometrical distancies ΔR_g for unknown compounds, in comparison to known ones, one can evaluate the k dependence of

$$\Delta R_g = \left[\Psi_{unk}(k) - \Psi_{kn}(k) \right]/2k \qquad (2)$$

where Π's are the arguments of the sine term in (1). Of course, one should find a constant value for ΔR_g as a sort of a plateau region.

As shown e.g. in ref. (24), to evaluate the coordination numbers one should know precisely all the terms influencing the amplitude. A way to extract the relative ratio $N_j unk/N_j$ kn, for two different structures is to calculate the quantity

$$\ln \frac{A_{unk}}{A_{kn}} = 2\ \Delta\sigma^2 k^2 + \frac{\Delta R_j}{\lambda} + \ln \left(\frac{N_{unk}}{N_{kn}} \quad \frac{R_{kn}^2}{R_{unk}}\right) \qquad (3)$$

with

$$\Delta\sigma^2 = \sigma_{kn}^2 - \sigma_{unk}^2$$

as a function of k^2. Formula (3) should give at least in a definite range of k^2 a straight line from which one can deduce N_{unk}/N_{kn} and $\Delta\sigma^2$, once known the quantities R_{unk}, R_{kn} and λ.

A second way is to compare the areas of corresponding shells between unknown and known samples in the Fourier transforms. By properly taking into account some corrections due to cut-off effects, one can deduce in such procedure both N_{unk}/N_{kn} and $\Delta\sigma^2$ provided that F(k) is not a too rapid function of k in the useful range.

There are many problems related to the Fourier transform technique. A major difficulty is the limitation in the k range values which can be used. This causes a broadening of the structures in the Fourier transforms, F(r), and interference between real peaks and cut-off effects.

For these reasons a great care should be put in data analysis in order to recognize possible artefacts.

3. - CRYSTALLOGRAPHIC PROPERTIES OF MODEL COMPOUNDS

In view of our investigation of more complex biological molecules, the model compounds used in our measurements are MnO and MnO_2 oxides where the Mn atoms are octahedrally coordinated by oxygen neighbours in the first shell.

The relevant crystallographic data for EXAFS analysis are reported in Table I for the two oxides[25].

Concerning the neighbours of Mn in the biological samples, where P atoms should be present, we used as reference compound MnP, which has the following relevant crystallographic properties (Table II).

TABLE I

	MnO_2			MnO		
shell	atom	d(Å)	C N.	atom	d(A)	C.N.
I	0	1,88	6	0	2 22	6
II	Mn	2,87	2	Mn	3,12	12
III	0	3,43	4	0	3,83	8

TABLE II

MnP			
shell	atom	d(A)	C.N.
I	P	2,35	6
II	Mn	2.80	6

4. - SAMPLE PREPARATION AND DATA ANALYSIS

The inorganic compounds were high purity products obtained from Merck and Alpha; Mn-ATP complexes were prepared by adding $Mn(ClO_4)_2$ to concentrated aqueous solutions 10% w/w of 5' Adenosine triphosphate (ATP) purchased from Boehringer Biochemia. No further purification was found to be necessary, the possible contamination from metal ions other than Mn having no practical importance due to the selectivity of the X-ray spectroscopy. The pH of each solution was adjusted to the desired value (3,7, or 9) before addition of Mn perchlorate. The ratio Mn:ATP was 1:1, 1:2, or 1:10, depending on pH, so that Mn-ATP complexes in very different conditions were obtained. The Mn-ATP solutions were divided in two parts: one was used to fill special teflon cells with Kapton windows. The other half were freeze-dried and then layered as a powder on a Kapton tape for a comparison of the results.

The sample thickness was chosen in order to obtain the better contrast at the K edge. The cells were 2÷10 mm thick, depending on the Mn concentration in the sample; a 0.5 M solution of $Mn(ClO_4)_2$ was also analyzed in a 1-mm thick cell. The inorganic model compounds were carefully layered (as powders) on a Kapton tape, obtaining thickness of about 5-10 mg/cm^2.

5. - EXPERIMENTAL APPARATUS

The experiment was made at the Synchrotron Radiation Facility at the Frascati Laboratories (PULS). Synchrotron radiation emitted by ADONE storage ring, working at 1.5 GeV, was monochromatized by a Si(220) channel-cut single crystal monochromator. The energy resolution at 7 keV was $\Delta E/E \sim 10^{-4}$. For XANES spectra the energy differences between two absorption peaks were accurate to ± 0.1 eV, where EXAFS spectra were collected with a ± 1 eV resolution. The experimental layout is shown in Fig. 3. Data acquisition and elaboration were done using a PDP/11 computer.

The zero energy of the photon energy scale for the XANES analysis has been taken at the first maximum of the derivate spectrum of metal Mn.

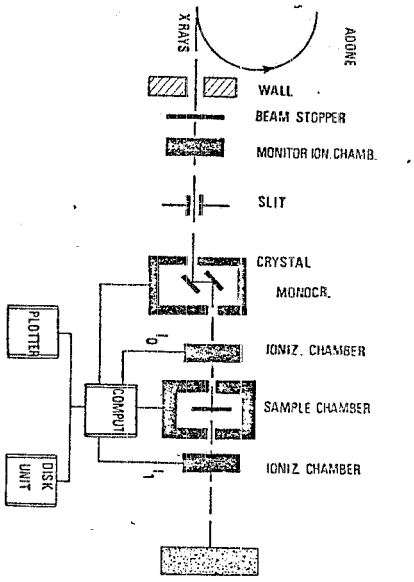

FIG. 3 - Experimental layout.

6. - EXPERIMENTAL RESULTS

6.1. - Model Compounds

We report in Fig. 4 the EXAFS spectrum of MnO_2, after background subtraction by means of a polynomial fit of the monotonous part of the absorption coefficient.

The Fourier transform of $k.\chi(k)$ reported in Fig. 5 shows three peaks. The analysis of the first peak by a

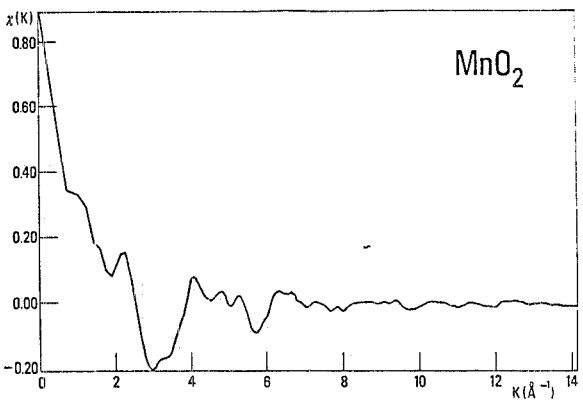

FIG. 4 - Oscillating part, $\chi(k)$, of the MnO_2 EXAFS spectrum.

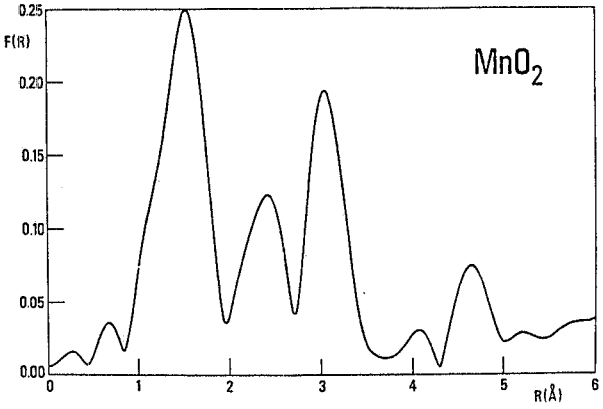

FIG. 5 - Fourier transform of $k\chi(k)$ for MnO_2 EXAFS spectrum.

back Fourier transform indicates the typical behaviour of the oxygen backscattering amplitude and the phases of Mn-O pair by a comparison with the expected values. In Fig. 6 the experimental phases are plotted for E_o equal to the flex point E_o=6530 eV in the edge of the absorption coefficient.

A similar analysis has been reported for MnO, which has a flex point of E_o=6550 eV. Data, also reported in

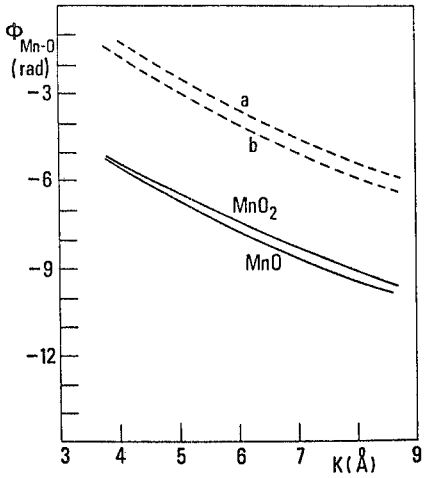

FIG. 6 - Phase shift of the Mn - O atom pair. Dashed lines: a) theoretical values from Ref. (21) and , b) solid lines experimental values found for MnO and MnO_2.

Fig. 6, confirm that the flex point gives the most convenient way for the choice of E_o.

In Fig. 7 we reported the Fourier transform of the EXAFS spectrum for MnO. Also in this case phase and amplitude of the back-Fourier transform are in agreement with the presence of oxygen atoms in the first shell.

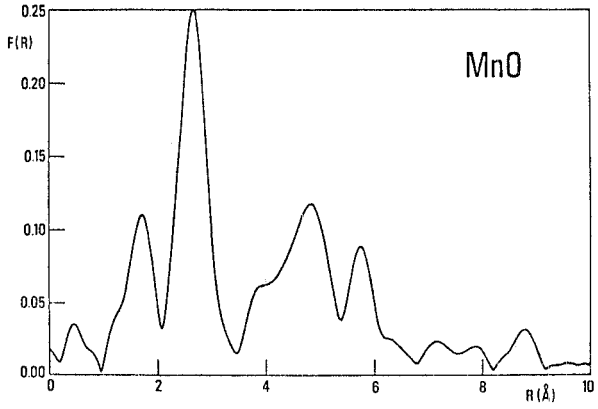

FIG. 7 - Fourier transform of $k\chi(k)$ for MnO EXAFS spectrum.

By comparing the experimental phase in the two compounds, we can be confident on the validity of phase transferability in our case, for which the formal charge on Mn in the model compound is the same as in the system we want to study.

As previously discussed, we determined the difference in the geometrical distances Mn-O in the two compounds. An agreement is found between the crystallographic and the measured value, $\Delta R_g = (0,32 \pm 0.02)\text{Å}$.

6.2. - Mn-ATP complexes

As both bond strenght and site structure in Mn-ATP complexes may depend on the pH value at which the complex was prepared, we made our analysis of X-ray spectrum on samples at three different pH values. The experimental conditions were also different for the stoichiometric proportions of Mn and ATP, in order to put in evidence the possible formation of different species of Mn-ATP complexes (including those where the N(7) of the adenine ring could be in the first shell neighbours of Mn). The complexes were obtained in the conditions reported in section 4 and a comparison was made of the spectra observed in aqueous solutions to the ones given by freeze-dried samples.

Fig. 8 and 9 report the Fourier transform of Mn ATP at three pH values, obtained for freeze-dried and liquid samples respectively.

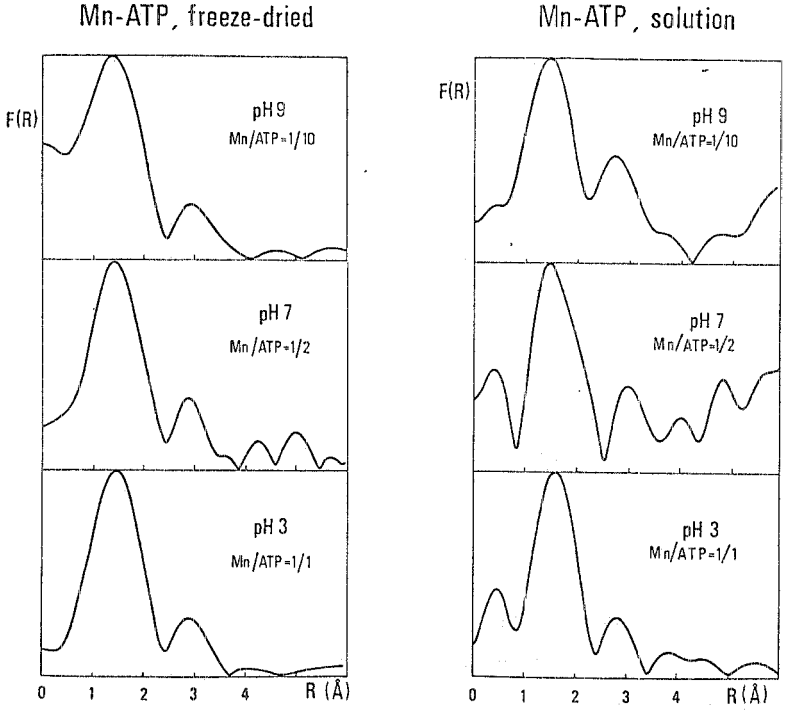

FIG. 8 - Fourier transform of $k\chi(k)$ for Mn-ATP freeze-dried samples, a) pH = 9, b) pH = 7, c) pH = 3.

FIG. 9 - Fourier transform of $k\chi(k)$ for Mn-ATP liquid samples; a) pH = 9, b) pH = 7, c) pH = 3.

6.3. - Edge analysis

Figs. 10 and 11 report the XANES spectra of different Mn-ATP complexes both for freeze-dried and liquid samples.

The relative absorption has been plotted, where μ_o is the value of the atomic absorption in the EXAFS region. Using this normalization, the monotonous part in the EXAFS region for all spectra overlap, allowing to compare the intensity of the peaks in the XANES region among different compounds.

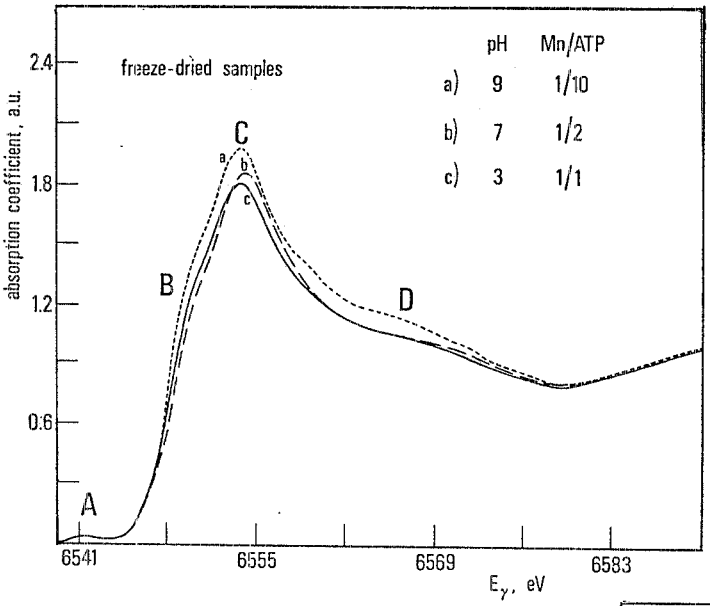

FIG. 10 - XANES spectra of freeze-dried Mn-ATP samples.

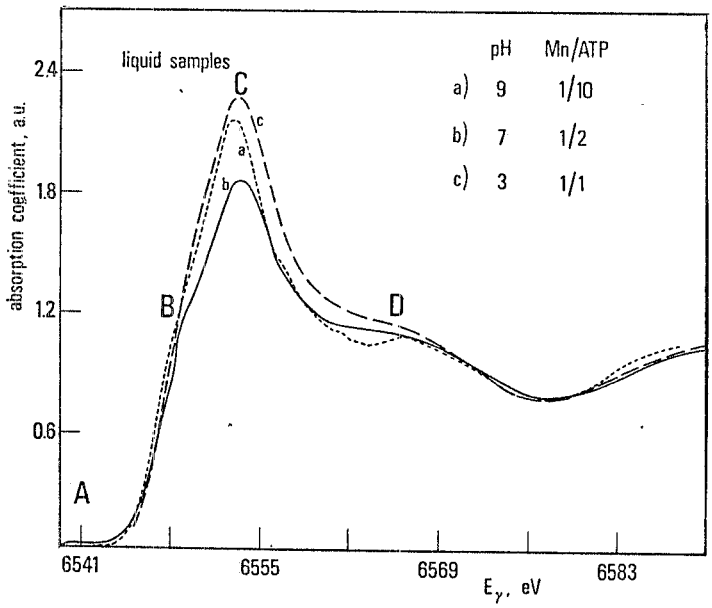

FIG. 11 - XANES spectra of liquid Mn-ATP samples.

7. - DISCUSSION

The Fourier trasforms show in Mn-ATP spectra two significant peaks and their back-Fourier analysis is consistent with the interpretation of the first peak as pure or mainly due to oxygen atoms. For the second shell the coordination numbers within the errors are consistent with N=6 which holds for MnO_2. The method does not appear enough sensitive to evidentiate one nitrogen atom in a shell made of many oxygens. By transferring the phase, as we said before, from model compounds MnO and MnO_2 to Mn-ATP samples, the distance R of the Mn-O

pair has been computed and plotted versus k, as it is shown in Figgs. 12 and 13. Results are reported in Table III for freeze-dried samples and Table IV for solutions. One can notice that the average distance of the first shell is

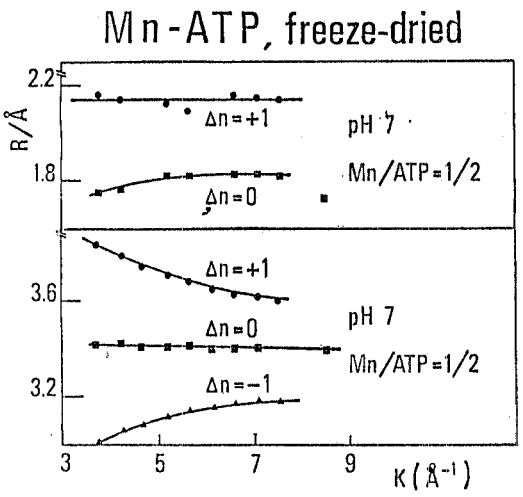

FIG. 12 - First and second shell radii vs k in freeze-dried Mn-ATP.

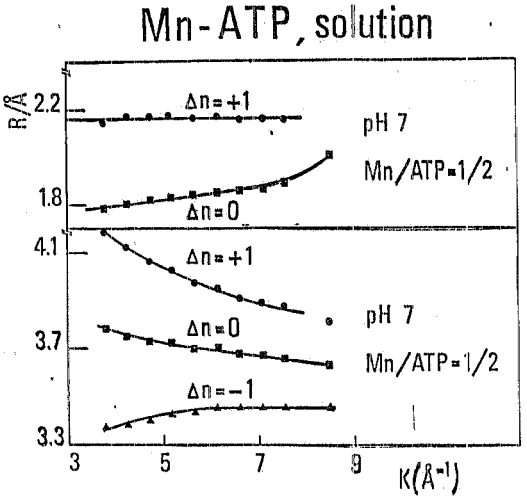

FIG. 13 - First and second shell radii vs k in liquid Mn ATP.

TABLE III - Freeze-dried samples.

Sample	1st shell		2nd shell	
	R(Å)	C.N.	R(Å)	C.N
Mn-ATP pH =3	2 10 ± 0.05	4 ± 1	3.4 ± 0.05	2 ± 1
Mn-ATP pH =7	2.14 ± 0.05	6 ± 1	3 4 ± 0.05	3 ± 1
Mn-ATP pH = 9	2.15 ± 0.05	6 ± 1	3.4 ± 0.05	3 ± 1

TABLE IV - Liquid samples.

Sample	1st shell		2nd shell	
	R(Å)	C.N.	R(Å)	C.N.
Mn- ATP pH = 3	2.15 ± 0.05	5 ± 1	3.4 ± 0.05	2 ± 1
Mn- ATP pH = 7	2.16 ± 0.05	4 ± 1	3.4 ± 0.05	4 ± 1
Mn- ATP pH = 9	2.15 ± 0.05	7 ± 1	3.3 ± 0.05	7 ± 1
Mn $(ClO_4)2$, aq. solut.	2.15 ± 0.05	5 ± 1		

almost the same for all compounds; it is also equal to the Mn-0 distance of the hydrated Mn ion, as observed in $Mn(Cl0_4)_2$ aqueous solutions.

The second shell peak has been interpreted as due to phosphorus atoms. The geometrical distances Mn-P have been found with the same procedure as for the first shell and are reported in Table IV. The values found for Mn-P distances are in good agreement with those quoted in ref. (26) for LiMn $P0_4$ crystals and in ref. (27) for metal-ATP complexes.

We also attempted a rough estimation of the coordination number both for the first and the second shell in all our samples. Results are given in the same Table III and IV, together with the indication of the estimated errors.

For the second shell the situation seems to be slightly different, because, at least in aqueous solutions, the coordination numbers of neighbouring P atoms around Mn increase for greater pH values. Our results are consistent with the experimental observation[10] that the negative charge of the phosphate groups increases as pH increases from 3 to 7.

The particularly high value for the coordination number of P atoms in the aqueous solution of Mn-ATP at pH9 may reflect the existence of intermolecular complexes such as dimers, in which one manganese atom binds to two ATP molecules (two triphosphate chains); this may be favoured by the low Mn:ATP ratio used (1:10). In fact dimeric molecules have been recently found in metal-ATP complexes[17]. The same indications are found in XANES analysis.

It can be worthwhile to observe that the average distance between the first shell oxygens and second shell phosphorus atoms is about 1.2 Å, which is smaller than the P-0 distance in the phosphate groups (~1.65 Å), in agreement with a geometry where the Mn-0 and 0-P bonds are not aligned.

A number of interesting conclusions can be drawn from the observation of near edge structures of the absorption spectra (Figs. 10 and 11).

In both liquid and freeze-dried samples the very low oscillator strenght associated with the pre-edge feature A is an indication that the Mn metal ion is in a centro-symmetric position. Indeed such a feature can be ascribed to the transition from the K-shell in Mn ion to an empty antibonding molecular orbital $\psi \sim \phi^{Mn}_{3d} - \lambda \phi^{0}_{2p}$ of 3d character on the metal ion and 2p character on the ligands.

Such a transition is parity forbidden in dipole approximation if the metal ion is in a centro-symmetric position with respect to the first coordination shell of the ligands. However it becomes weakly allowed in quadrupole approximation, the intensity being about a factor 100 smaller than the dipole allowed first strong absorption maximum (peak C in Fig. 10).

Theoretical and experimental evidence bears this out (Refs. (28),(29)).

Now, examination of the pre-edge feature A in Mn-ATP spectra seems to exclude, in the light of the preceeding considerations, the presence of a N-atom of the adenine ring in the first coordination shell of the metal-ion as substitutional for an O-atom in the octahedron of oxygen ligands around the Mn metal ion. Indeed, the intensity ratio between peaks A and C is of the same order of magnitude as the ratios between the same absorption features in the series $KMnF_3$, $KFeF_3$, $KCoF_3$, $KNiF_3$, all of them known to have the fluorine ligand atoms octahedrally coordinated around the transition metal ion. (cfr. Ref. (28)) where it is also shown that peak A is absent in $KZnF_3$, since the Zn 3d shell is full. The same is true for CuCl and $CuCl_2$[29] where the quadrupolar character of the transition is actually demonstrated by angular measurement with polarized light.).

If a N-atom were substitutionally present in the first coordination shell of the O-ligands, it would break the inversion symmetry around the metal ion, making the transition to the 3d antibonding molecular states dipole allowed with an intensity which is estimated in the Appendix to be at least a factor one to two higher than the quadrupole allowed one. This latter would be always present, so that the intensity of peak A would be expected to double or triple. (In the same Appendix, the possibility is discussed that a substitutional N-atom might be directly

coordinated to the metal ion in MnAMP complexes).

Looking now at the liquid samples spectra (Fig. 11) we observe that feature D becomes more and more pronounced with increasing pH (from 3 to 9). There are experimental as well as theoretical reasons to believe that this feature is associated with the second shell coordination atoms, being more pronounced the higher is the scattering power of the second neighbours.

Experimentally (Ref. (30)) this is borne out by the edge spectra of $MnHPO_4$, Mn-AMP, Mn-ATP and $Mn_2P_2O_7$ (Fig. 14). There is an apparent correlation between the number of second P-atoms neighbors and the intensity of feature D.

On the theoretical side (Ref. (31)) one can establish a rough correlation between the order in which a particular peak is met in the spectrum with increasing energy, starting from the first strong absorption maximum, and the order of the shell contributing to it this correlation becoming weaker and weaker the higher the order of the peak.

This finding for liquid samples is in keeping with the result obtained by EXAFS analysis, which shows an increasing coordination number of P-atoms around Mn with increasinf pH, pointing to a complex formation of Mn with two ATP molecules at pH=9 (Table IV).

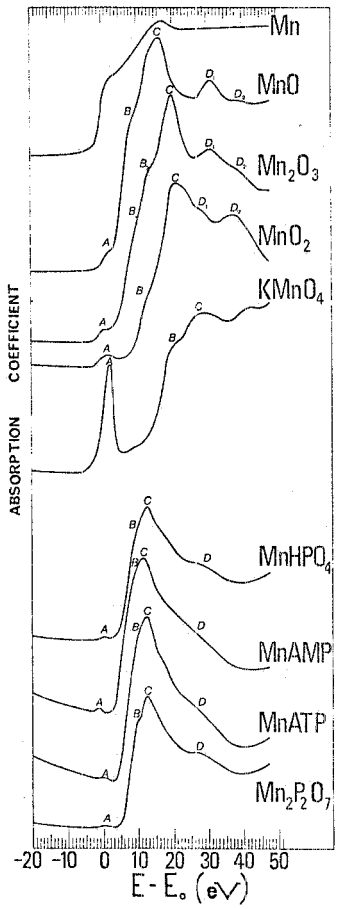

FIG. 14 - X-ray absorption coefficient vs photon energy difference E-Eo where Eo is the zero of the photon energy scale taken at the first maximum of the derivative spectrum of the metal Mn.

In freeze-dried samples (Fig. 10) such an effect is not observed. In all three cases (pH=3, 7, 9) features D are not very well pronounced and similar in shape indicating that the second shell coordination around Mn is very much alike in the three samples.

Again this finding is in agreement with the results of EXAFS analysis for the second coordination shell in Table III, where the number of second neighbors P-atom is 3 at pH= 9 and 7 and 2 at pH= 3.

These results seems to indicate that coordination of the Mn metal ion to one ATP molecules is the most stable configuration, which takes place under a wide variety of thermodynamical conditions. The dimer complex instead can be thought of as a state that is formed only at room temperature and pH = 9 because of the high ratio of ATP molecules to Mn atoms (10 to 1), but as soon as the solution is freeze-dried the usual monomeric configuration is recovered through retention of water molecules.

Finally in both liquid and freeze-dried samples peak C at pH= 9 is shifted to lower energy (0.4 ± 0.2 eV) compared to the case pH= 7.

Theoretical considerations (Ref. (31)) suggest that the variation in energy of the first strong absorption maximum (peak C) is mainly related to a variation in distance of the first coordination shell around the metal ion, the relation being

$$\frac{\Delta \bar{E}_r}{2\bar{E}_r} = - \frac{\Delta R}{R}$$

where $\bar{E}_r$ is the energy of the maximum referred to a "muffin tin" zero of the molecular cluster, estimated to lie 4 eV below peak A. Putting in numbers, we derive that the Mn-O distance increases with increasing pH, ΔR being of the order of 0.03 Å.

This indicates, as expected, a slight increase of covalency of the Mn-O bond with increasing pH, as suggested by the trend observed in the series Mn, MnO, Mn_2O_3, MnO_2, $KMnO_4$ in Fig. 14, where the Mn-O distance decreases with increasing ionicity (or decreasing covalency).

CONCLUSIONS

We can draw from our data the following conclusions:

1) The Mn metal ion is in centro-symmetric position in the Mn ATP complexes, octahedrally coordinated to the oxygen ligands.
2) The first and second shell distances appear the same in all the samples, being equal to (2.15 ± 0.05) Å and (3.40 ± 0.05) Å respectively.
3) The presence of a N-atom of the adenine ring in the first coordination shell seems to be excluded.
4) A $Mn(ATP)_2$ = 1:2 complex is formed in solution at pH=9 at room temperature, while the Mn:ATP 1:1 complex is the most stable configuration under all other conditions.
5) A small increase of covalency in the Mn-O bond occurs with increasing pH.

ACKNOWLEDGEMENTS

We thank Dr. A. Werner for his helpful suggestions in the EXAFS analysis of data during his one month stay at LNF.

Thanks are also due to all the members of the staff of the synchrotron radiation laboratory and the Adone machine group at LNF.

We are indebted to Mr. F. Notargiacomo for technical assistance in sample preparation, and to Mrs. L. Invidia for her skill and patience in typing the manuscript and its revisions.

APPENDIX

We describe a simple octahedral complex of a 3d transition metal ion of the type ML_6^{n-} (where M indicates the metal and L the ligand) in the framework of the molecular orbital bonding model. A useful resumé of this model is contained in a review article by B.C. Toefield (Ref. (32) and references therein) on the study of covalency by magnetic neutron scattering.

For our purposes of estimating the oscillator strenght of the transition from the K-shell of metal ion to an empty molecular orbital in an octahedral complex when one oxygen ligand is replaced by a nitrogen atom, we shall have to consider only antibonding orbitals.

For a MnO_6^{10-} complex where Mn has a formal valence of 2 (configuration $3d^5$) the antibonding states of Eg type (twofold orbitally degenerate) and T_{2g} type (threefold orbitally degenerate) are occupied by two and three electrons respectively with parallel spins (molecular complex configuration $T_{2g}^3 E_g^2$).

The E_g states, of σ bonding character, can be written as

$$\psi_\sigma = N_\sigma (\phi_{3d\sigma} - \lambda_\sigma \chi_{2p\sigma} - \lambda_s \chi_{2s}) \tag{A1}$$

whereas the T_{2g} states of π bonding character, can be represented as

$$\psi_\pi = N_\pi (\phi_{3d\pi} - \lambda_\pi \chi_{2p\pi}) \tag{A2}$$

In these equations, $N_{\sigma,\pi}$ are normalization constants, χ_{2s}, $\chi_{2p\sigma}$, $\chi_{2p\pi}$ are appropriate linear combinations of ligand 2s, 2pσ and 2pπ orbitals transforming according to the E_g and T_{2g} representation of the point group O_h of the molecular complex. Written in full, the E_g functions read

$$\psi_{z^2} = N_\sigma \left[\phi_{3dz^2} - \frac{1}{\sqrt{12}} \lambda_\sigma (-2P_{z3}+2P_{z6}+P_{x1}-P_{x4}+P_{y2}-P_{y5}) + \right.$$
$$\left. - \frac{1}{\sqrt{12}} \lambda_s (2S_3+2S_6-S_1-S_2-S_4-S_5) \right] \tag{A1'}$$
$$\psi_{x^2-y^2} = N_\sigma \left[\phi_{3dx^2-y^2} - \tfrac{1}{2} \lambda_\sigma (P_{x4}-P_{x1}+P_{y2}-P_{y5}) - \tfrac{1}{2} \lambda_s (S_1+S_4-S_2-S_5) \right]$$

whereas the T_{2g} functions read

$$\psi_{xy} = N_\pi \left[\phi_{3dxy} - \tfrac{1}{2} \lambda_\pi (P_{y1}-P_{y4}+P_{x2}-P_{x5}) \right]$$
$$\psi_{yz} = N_\pi \left[\phi_{3dxz} - \tfrac{1}{2} \lambda_\pi (P_{z2}-P_{z5}+P_{y3}-P_{y6}) \right] \tag{A2'}$$
$$\psi_{yz} = N_\pi \left[\phi_{3dyz} - \tfrac{1}{2} \lambda_\pi (P_{x3}-P_{x6}-P_{z1}-P_{z4}) \right]$$

where, e.g. P_{xj} represents the ligand 2p w.f. at site j, pointing along x axis, the sites being numbered so that ligands 1, 2, 3 are located on the positive x, y, z axes, and 4, 5, 6 on the negative x, y, z axes respectively (Ref. (32)).

When a N-atom replaces substitutionally one of the O-ligands in the octahedral cage around the metal ion at site j, the corresponding w.f. can be written as

$$\psi_\sigma = N_\sigma (\phi_{3d\sigma} - \lambda^0_\sigma \chi_{2p\sigma} - \lambda^0_s \chi_{2s}) - \frac{m}{\sqrt{n}} N_\sigma \left[(\lambda^N_\sigma \phi^N_{2p\alpha j} - \lambda^0_\sigma \phi^0_{2p\alpha j}) - (\lambda^N_s \phi^N_{2s\alpha j} - \lambda^0_s \phi^0_{2s\alpha j}) \right] \quad \text{(A3a)}$$

$$\psi_\pi = N_\pi (\phi_{3d\pi} - \lambda^0_\pi \chi_{2p\pi}) - N_\pi \frac{m'}{\sqrt{n'}} (\lambda^N_\pi \phi^N_{2p\alpha j} - \lambda^0_\pi \phi^0_{2p\alpha j}) \quad \text{(A3b)}$$

where $\phi^N_{2p\alpha j}$ represents the nitrogen 2p w.f. pointing along the α axis (α=x, y, z) at site j and $\frac{m}{\sqrt{n}}$ is the appropriate coefficent as can be derived from Eqs. (A1'), (A2').

The total oscillator strenght for transitions from the K-shell metal ion to antibonding states is proportional to

$$\left[\frac{N^2_\sigma}{3} (\lambda^N_\sigma + \lambda^N_s - \lambda^0_\sigma - \lambda^0_s)^2 + \frac{N^2_\pi}{2} (\lambda^N_\pi - \lambda^0_\pi)^2 \right] \left| (\phi^N_{2p} | \; r \; | \phi^{Mn}_{1s}) \right|^2 \quad \text{(A4)}$$

having summed over all E_g and T_{2g} states. As can be inferred from the expressions (A1') (A2') the result is independent of the particular substitutional site j, since e.g. $\Sigma_{E_g} \frac{m^2}{n} = \frac{1}{3} = \frac{4}{12} = \frac{1}{12} + \frac{1}{4}$, $\Sigma_{T_{2g}} \frac{m'^2}{n'} = \frac{1}{2} = \frac{1}{4} = \frac{1}{4}$. Also we have assumed that $\left| (\phi^N_{2p} | \, r \, | \phi^{Mn}_{1s}) \right| \sim \left| (\phi^0_{2p} | \, r \, | \phi^{Mn}_{1s}) \right|$ as an order of magnitude.

Since we have been unable to find in the literature the covalency admixture parameters $\lambda^N_{\sigma,\pi}$ relative to the Mn-N bond, we have estimated them on the basis of the electronegativity scale.

From Ref. (32) we know the covalency parameters for the Mn-F and Mn-O bonds, as derived from neutron spin density measurements and NMR measurements on the ligand atoms.

Using the fact that the electronegativity difference ($x_F - x_0 = 0.5$) between F and O is the same as between O and N ($x_0 - x_N = 0.5$), remebering that $\lambda^2_{\sigma,\pi,s}$ relates to the charge transfer from ligands to the metal ion, we derive that

$$(\lambda^N_{\sigma,\pi,s})^2 - (\lambda^0_{\sigma,\pi,s})^2 = (\lambda^0_{\sigma,\pi,s}) - (\lambda^F_{\sigma,\pi,s})^2 \quad \text{(A5)}$$

under the assumption that each λ^2 scales linearly with electronegativity, which is plausible for small electronegativity changes.

Table AI summarizes the λ values for the various bonds.

TABLE AI

	Mn-F	Mn-O	Mn-N
λ_s	0.12 ± 2.10^{-4}	0.15 ± 2.10^{-4}	0.18
λ_σ	0.18 ± 0.04	0.21 ± 0.04	0.24
λ_π	0.18 ± 0.05	0.17 ± 0.05	0.15

It is fair to say that these λ values for Mn are anomalously low compared to other ions in the first row of the transition metal series, probably because in the interpretation of the experimental neutron data no account has been taken of the polarization of the 4s electrons by the high spin $3d^5$ configuration of the Mn metal ion, which tends to reduce the magnetic moment as measured by neutrons. Indeed direct calculations of the λ parameters for Mn fluorides and oxides tend to give higher values of the covalency parameters and to produce a more marked difference between fluorides and oxides.

Therefore we calculate expression (A4) using the values of Table AI, keeping in mind that this estimate represents a lower bound to the true value.

Inserting numbers, we obtain that the oscillator strenght is proportional to

$$\left[\frac{N_\sigma^2}{3} \cdot 36 + \frac{N_\pi^2}{2} \cdot 4\right] \cdot 10^{-4} \left|(\phi_{2p}^N \mid r \mid \phi_{1s}^{Mn})\right|^2 \qquad \text{(A6)}$$

An idea about the intensity to be expected in such a transition can be obtained if we compare (A6) with the strenght of the first peak in $KMnO_4$ (Fig. 14), which is given by

$$4N_\sigma^2 (\lambda_\sigma^{T_d})^2 \left|(\chi_{2p}^0 \mid r \mid \phi_{1s}^{Mn})\right|^2 \lesssim 4N_\sigma^2 (\lambda_\sigma^{T_d})^2 \left|(\phi_{2p}^0 \mid r \mid \phi_{1s}^{Mn})\right|^2 \qquad \text{(A7)}$$

where χ_{2p}^o is the combination of Oxygen 2p w.f. transforming according to the T_2 representation of the tetrahedral group T_d and $\lambda_\sigma^{T_d}$ is the covalency admixture parameter for tetrahedral coordination. We observe that the intensity of this transition is comparable to the intensity of the first strong absorption maximum (peak C).

If we take for $\lambda_\sigma^{T_d}$ the same value as for the octahedral complex λ_σ^{On} we get for the ratio of the two oscillator strenghts the value

$$r = \frac{14 \cdot 10^{-4}}{4 \cdot 21^2 \cdot 10^{-4}} \sim 10^{-2} \qquad \text{(A8)}$$

assuming $N_\sigma^2 \sim N_\pi^2 \sim 1$, which is plausible for λ values $\ll 1$.

In other words the weakly parity allowed transition in the $Mn\ O_5N^{-10}$ complex has an oscillator strenght of the same order of magnitude as the quadrupole allowed transition to 3d antibonding states in the octahedral complex $Mn\ O_6^{10-}$, which is about one hundredth of the transition associated with peak C.

We then conclude that the intensity of peak A should at least double in going from $Mn\ O_6^{10-}$ to $Mn\ O_5N^{10-}$. Also a slight slift in the energy position of the peak is expected due to the slight difference in electronegativity between O and N.

At this point some considerations are in order about the values in Table AI used for the covalency parameters. These values, derived from spin density measurements by neutron scattering and NMR techniques on ligands are pertinent to the ground state of the complex without the inner core hole on the metal ion, whereas in X-ray absorption edge measurements the system in its final state is relaxed around the core hole. Consequently the covalency admixture parameters should be relative to the relaxed final state.

Now in first order perturbation theory λ is given by

$$\lambda = \frac{(\phi_{3d} \mid h \mid \chi_{2p})}{E_{3d} - E_{2p}} \qquad \text{(A9)}$$

where h is an effective one particle hamiltonian (h=T+V). The effect of the relaxation is to decrease the difference $E_{3d}-E_{2p}$ and to increase the value of the matrix element $(\phi_{3d} \mid h \mid \chi_{2p})$, since the potential becomes deeper on the side of the metal ion.

Hence as a general rule we infer that in the relaxed final state the values increase as also the difference $\lambda^N - \lambda^0$ does.

As a result it is not unreasonable to expect an increase of the estimate of the ratio in Eq. (A8) by a factor of two or so.

Such an increase in intensity of peak A as well as a slight shift toward lower energies is actually what is observed in Mn-AMP spectra as compare to Mn-ATP spectra.

This fact might indicate in the MnAMP complex the presence of a N atom of the adenine ring in the first coordination shell of Mn, as opposed to the case of Mn ATP complex where only O-atoms should be present.

Since the effect is a small one after all, such an interpretation should await further confirmation from a cluster calculation of the two complexes and more careful analysis of the experimental spectra to be taken under more favourable conditions around peak A.

REFERENCES

(1) P. Eisenberger, R.G. Shulman, B.M. Kincaid, G.S. Brown and S. Owaga, Nature 274, 30 (1978).
(2) M. Daune in "Metal Jons in Biological Systems"; H. Sigel Ed. 3, 1-39 (1974).
(3) I. Sissöef, J. Grisvard, E. Guillé, Prog. Biophys. Molec. 31, 165 (1976).
(4) M. Daune, Studia Biophys. 24, 287 (1970).
(5) K. Bruce Jacobson, J.E. Turner, Toxicology 16, 1 (1980).
(6) J. Karlik, G.L. Eichhorn, P.N. Lewis and D.R. Crapper, Biochemistry 19, 5991 (1980).
(7) B. Rosemberg, L. Van Camp, J.E. Trosko and V.H. Mansour, Nature, 222, 385 (1969).
(8) S. Kominami, V.T. Wee and P. Riesz, Radiat Res. 62, 422 (1975)
(9) G.L. Eichhorm, N.A. Berger, J.J. Butzon, P. Clark, J. Heim, J. Pitha, C. Richardson, J.M. Rifkind, Y. Shin and E. Tarien, Adv. Exp. Med. and Biol., 40, 43 (1974).
(10) See for a review, R.B. Martin, Y.H. Mariam in "Metal ions in biological systems", H. Siegel Ed. 8, 57 (1979).
(11) A. Szent-Györgyi, "Bioenergetics", Acad. Press Inc. New York (1957).
(12) H. Sternlicht, R.G. Shulman, E.W. Anderson, J. Chem. Phys. 43, 3123 (1965).
(13) H. Sternlicht, R.G. Shulman, E.W. Anderson, J. Chem. Phys. 43, 3133 (1965).
(14) T.A. Glassman, C. Cooper, L.W. Harrison, T.J. Swift, Biochemistry 10, 843 (1971).
(15) Y.F. Lam, G.P.P. Kuntz, G. Kotowycz, J. Am. Chem. Soc. 96, 1834 (1974).
(16) R. Basosi, N. Niccolai, E. Tiezzi, G. Valensin, J. Am. Chem. Soc. 100, 8047 (1978).
(17) W. Wee, I. Feldman, P. Rose, S. Gross, J. Am. Chem. Soc. 96, 103 (1974).
(18) R. de L. Kronig, Z. Phys. 70, 317 (1931); E. Sayers, E.A. Stern, F.W. Lytle; Phys. Rev. 11, 4836 (1975).
(19) See for a review P.A. Lee, P.M. Citrin, P. Eisenberger and B.M. Kincaid; Review of Modern Physics 53, 769 (1981).
(20) A. Bianconi, S. Doniach and D. Lublin; Chem. Phys. Letters 59, 121 (1978).
(21) B.K. Teo and P.A. Lee; J. Am. Chem. Soc. 101, 2815 (1979).
(22) E.A. Stern; Phys. Rev. B10, 3027 (1974); P.A. Lee and G. Beni; Phys. Rev. B15, 2862 (1977).
(23) P. Eisenberger, R.G. Shulman, G.S. Brown and S. Ogawa; Proc. Natl Acad. Sci. USA 73, 49 (1976).
(24) P. Rabe, G.T. Tolkien and A.W. Werner; J. Phys. C Solid State Phys. 12, 1173 (1979).
(25) R.W.G. Wyckoff; Crystal Structures, Interscience (1948).
(26) S. Geller and J.L. Duran; Acta Crystallog. 13, 325 (1960).
(27) M. Sundaralingam; Biopolymers 7, 821 (1969).
(28) R.J. Shulman, Y. Yafet, P. Eisenberger and B. Blumberg; Proc. Natl. Acad. Sci. USA 73, 1384 (1976).
(29) J.E. Hahn, R.A. Scott, K.O. Hodgson, S. Doniach, S.R. Dejardins and E.J. Solomon; Chem. Phys. Letters 88, 595 (1982).
(30) M. Belli, A. Bianconi, E. Burattini, S. Mobilio, L. Palladino, A. Reale and A. Scafati; Solid StateCommun. 26, 500 (1980).
(31) C.R. Natoli "Near edge absorption structures in the framework of the multiple scattering model", Proc. of the Inter. Conf. of EXAFS and Near Edge Structures, Frascati (1982), Chemical Physics Series, Springer Verlag, Berlin (to be published).
(32) B.C. Tofield; "Structure and Bonding, Springer Verlag, Berlin Heidelberg N.Y. (1975).